

ENERGY YIELD MODELLING OF 2D AND 3D CURVED PHOTOVOLTAIC MODULES

Sebastian Neven-du Mont*, Martin Heinrich, Andrea Pfreundt, Christoph Kutter, Ammar Tummalieh, Holger Neuhaus
 Fraunhofer Institute for Solar Energy Systems ISE
 Heidenhofstraße 2, 79110 Freiburg, Germany

*Corresponding Author: +49 761 4588 2282, sebastian.neven-du.mont@ise.fraunhofer.de

ABSTRACT: This paper presents a detailed model to simulate the energy yield potential of various designs of curved PV modules depending on their bending angle, orientation and location. Furthermore, we analyze the effective irradiance incident on the curved cell pattern surface to investigate the current mismatch between cells and strings that results from the deviating level of irradiance reaching the cells. The results of our simulations show that parallel interconnection of strings produces a higher energy yield for most but not all curved module layouts compared to standard series interconnection with three bypass diodes. The energy yield of curved PV modules can be maximized by using an adapted module design that compensates the inhomogeneous irradiance distribution on the curved module surface.

Keywords: curved PV modules, BIPV, VIPV, energy yield, inhomogeneous irradiance, interconnection topology

1 INTRODUCTION

Photovoltaic (PV) modules in curved variations are a solution to overcome three-dimensional shapes in buildings or other structures to more effectively meet building integrated (BIPV) [1, 2] and vehicle integrated photovoltaic (VIPV) [3–5] application requirements. However, fabrication and especially performance prediction of such modules is significantly more complex compared to planar modules.

The incidence angle of radiation reaching the surface of PV modules has a major influence on module power. In curved PV modules the incidence angle varies across the module surface which causes current mismatch between cells and strings. In this paper, we have simulated the irradiance distribution over two-dimensional (2D) and three-dimensional (3D) curved surfaces of 60-cell modules with different angles of curvature.

The purpose of this work is to evaluate the influence of cell pattern curvature on the irradiance distribution over curved surfaces averaged for typical solar cell formats considering the incidence angle of the sun. Furthermore, we developed an analytical model to analyze the influence of the module curvature on the yearly energy yield. Light attenuation effects such as cover reflection and path length dependent absorption are not considered. Our model extends previous work on 2D curved PV modules [6] by considering curvature not only in one but two directions (3D curved modules). This extension is necessary particularly with regard to VIPV applications where PV has to follow 3D contours.

A number of studies have been conducted worldwide concerning irradiance on curved modules for VIPV applications [6–12] yet this is the first scientifically accurate approach to calculate the impact of inhomogeneous insolation of the 3D curved module surface on the power output and the yearly yield.

3 THEORY

An analytical model based on a previous publication [6] is developed to simulate the optical characteristics of 2D and 3D curved modules depending on their location and their level of curvature.

3.1 Calculation of Radiation Power on Curved PV Modules

The curvature of PV modules can be characterized using the tilt angle ω between the center of neighboring cells as shown in Fig. 1.

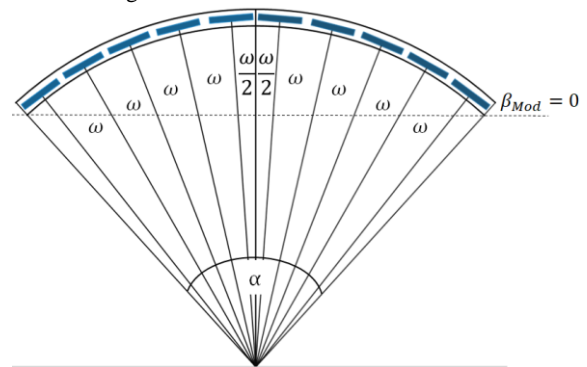


Figure 1 Curved module with $\omega = 8^\circ$ tilt between the cells over the 10-cell axis, module bending angle α and module tilt angle $\beta_{Mod} = 0$ [6]

Figure 2 illustrates the position of the sun relative to a cell where α_s is the elevation angle and γ_s the azimuth of the sun which are dependent of the location, date and time. By definition, the azimuth is 0° for the north direction, 90° for east, 180° for south and 270° for west [13].

The elevation angle α_s is 0° for the horizontal case and 90° when the sun is at its zenith.

In 3D curved modules the integrated cells are tilted in two directions. $\beta_{C,X}$ represents the tilt angle of the individual cell along the 10-cell axis and $\beta_{C,Y}$ the tilt angle along the 6-cell axis. γ_C describes the cell's azimuth.

In 2D curved modules the surface is bend solely over one axis, hence one of the tilt angles equals zero.

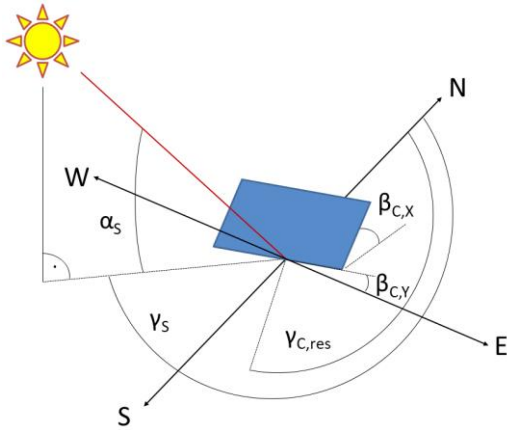


Figure 2 Position of the sun relative to a point on a cell integrated in a 3D curved module

The resulting angle going through the center of each cell is calculated via:

$$\beta_{C,res} = \cos^{-1}(\cos(\beta_{C,x}) \cdot \cos(\beta_{C,y})) \quad (2)$$

The azimuth angles of cells in 3D curved modules with $\beta_{Mod} = 0$ can be derived from the calculation of the azimuth angle of the first quarter ("1" in Fig. 3) for symmetry reasons.

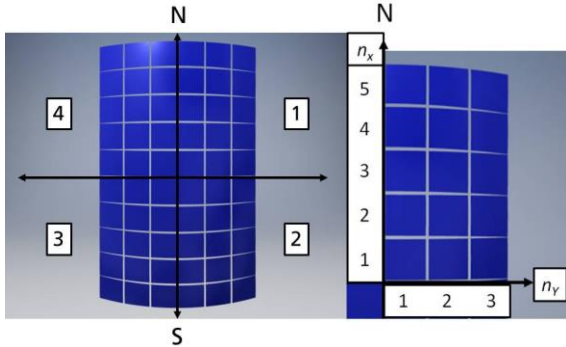


Figure 3 left: 3D curved PV module with orientation; right: upper right quarter with description of n_x and n_y

The azimuth angle is approximated by:

$$\gamma_{C,res} = \tan^{-1} \left(\frac{\left(\frac{b_y \cdot 360}{\pi \cdot \alpha_y} \right) \cdot \sin\left(\frac{\alpha_y}{2}\right)}{\left(\frac{b_x \cdot 360}{\pi \cdot \alpha_x} \right) \cdot \sin\left(\frac{\alpha_x}{2}\right)} \right) \quad (3)$$

With

$$\alpha_x = \left(\frac{\omega_x}{2} \right) + (n_x - 1) \cdot \omega_x \quad (4.1)$$

$$\alpha_y = \left(\frac{\omega_y}{2} \right) + (n_y - 1) \cdot \omega_y \quad (4.2)$$

b_x is the arc length in the-direction of the 10-cell axis from the center of the module to the center of the cell for a standard 60-cell module and b_y is the arc length in 6-cell axis direction respectively. n_x and n_y indicate the cell counting from the midpoint of the module as shown in Fig. 3.

The irradiance incident on a cell in a 3D curved module can now be calculated according the equation:

$$I_{cell} = \frac{GHI}{\sin \alpha_s} \cdot \left[\cos(\alpha_s) \cdot \sin(\beta_{C,res}) \cdot \cos(\gamma_C - \gamma_s) + \sin(\alpha_s) \cdot \cos(\beta_{C,res}) \right] \quad (5)$$

where I_{cell} is the radiation power density reaching the cell and GHI is the global horizontal irradiance reaching the module.

2 METHODOLOGY

Figure 4 depicts the approach for the energy yield simulation for various designs of 2D and 3D curved PV modules.

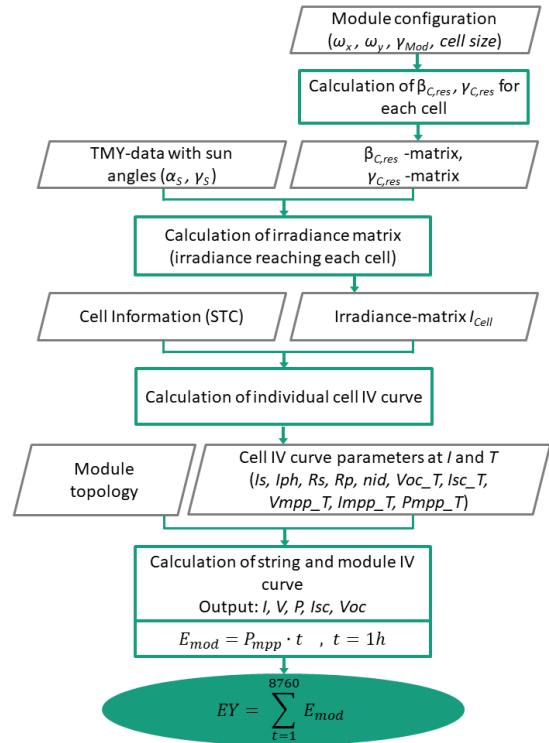


Figure 4 Methodology Energy Yield Simulations

For our simulations we use a Typical Meteorological Year Dataset (TMY) from Solcast API [14] to calculate the energy yield of different 2D and 3D curved module-layers. The dataset has been produced by choosing for each month the most "typical" month out of 11 years of data (2007–2018) [14]. The sun angles (elevation and azimuth) are calculated for each hour of the year by using MATLABs PVLIB toolbox [15].

At first, parameters describing the module configuration are determined to calculate each cells individual tilt and azimuth angle in the center of the cell.

The irradiance reaching each cell is calculated with Eq. (5) by using the TMY-Dataset containing the sun angles (α_s , γ_s), global horizontal irradiance GHI for each hour of the year, the individual cell tilt angle $\beta_{C,res}$ and azimuth angle $\gamma_{C,res}$.

We calculate the individual cell IV curves with respect to cell temperature T_{cell} and cell irradiance I_{cell} with SmartCalc.IV [16] by using the irradiance-matrix and the cell information (Cell IV parameters at STC) for every cell summarized in Table I.

Table I Cell parameters at STC

Cell parameters	Values
Cell Format	156.75 x 156.75 cm ² (M2)
V _{oc}	0.671 V
I _{sc}	9.693 A
V _{mpp}	0.571 V
I _{mpp}	9.206
Temperature coefficient V _{oc}	-0.0029 %/K
Temperature coefficient I _{sc}	0.0004 %/K
T _{Cell}	25°C
N _S	1

We compare standard 60-cell modules with series interconnection with three bypass diodes and parallel interconnection of strings as illustrated in Fig. 5 to analyze the influence of the interconnection topology on the energy yield for each level of module curvature.

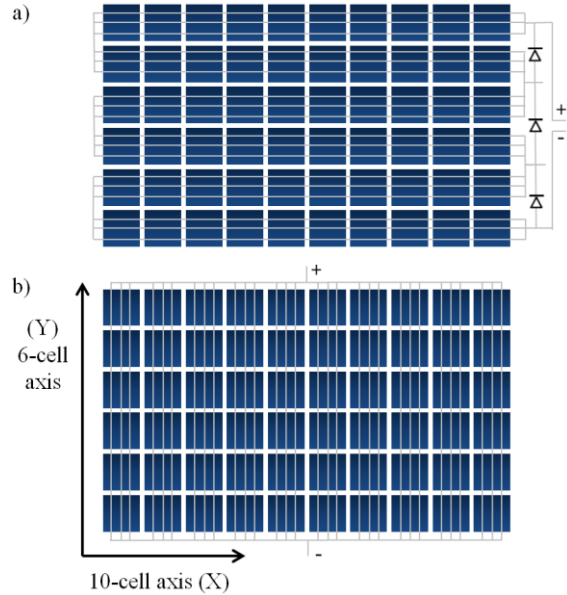


Figure 5 (a) Module Topology with series interconnection and three bypass diodes (b) Module Topology with parallel interconnection

The calculation of the string and module IV curves is based on IV curve addition. Our model for cell, string and module IV curve calculation will be explained in more detail in a future publication [16].

The module power at maximum power point is taken as reference power for the energy yield calculations as depicted in Fig. 4. The module bending angle α of the investigated 2D curved PV modules is varied between 0 degrees ($\omega_{x,y} = 0^\circ$) and 80 degrees ($\omega_x = 8^\circ$) for the 10-cell axis and 48 degrees ($\omega_y = 8^\circ$) for the 6-cell axis respectively, as indicated in Fig. 6.

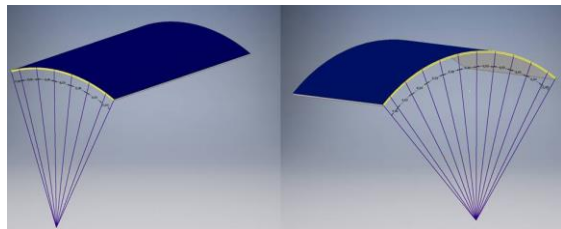


Figure 6 left: 2D module curvature over the 6-cell axis. right: 2D module curvature over the 10-cell axis with $\omega = 8^\circ$ tilt between the cells

The simulations are done for the module configurations shown in Table II. All simulations are done for a Location 48° N and 7.85° E of prime meridian (Freiburg, Germany) and all modules are facing south ($\gamma_{Mod} = 180^\circ$). Electrical losses are not considered in these calculations.

Table II Module configurations for EY Simulations

Module type	Index	Tilt angle between cells		Module bending angle	
		$\omega_x [^\circ]$	$\omega_y [^\circ]$	$\alpha_{x,t} [^\circ]$	$\alpha_{y,t} [^\circ]$
Standard module	REF	0	0	0	0
2D curved modules	X2Y0	2	0	20	0
	X8Y0	8	0	80	0
	X0Y2	0	2	0	20
	X0Y8	0	8	0	48
3D curved modules	X2Y2	2	2	20	12
	X2Y8	2	8	20	48
	X8Y2	8	2	80	12
	X8Y8	8	8	80	48

4 RESULTS

4.1 Radiation power density on 2D curved PV modules

In a first step, we calculate the radiation power density reaching each cell in curved PV modules at Standard Testing Conditions (STC) (1000 W/m² perpendicular to the center of the module at $T_{amb} = 25^\circ\text{C}$) to analyze the mismatch inside 2D and 3D curved PV modules at best condition.

Figure 7 shows the irradiance for different tilt angles at the center of each cell in a string which varies due to the two-dimensional module curvature. As the produced current is proportional to the irradiance reaching the cells it can be concluded that for tilt angles higher than 8° current mismatch > 20 % can be observed within a string in series interconnection.

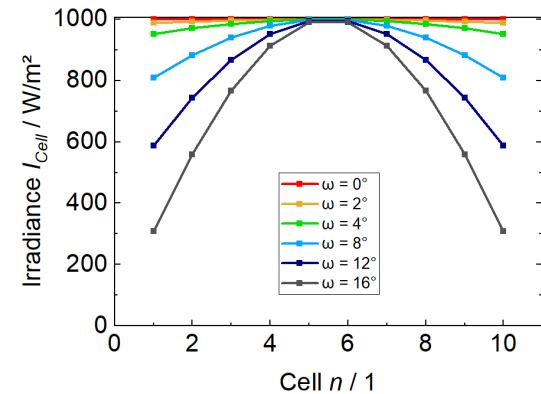


Figure 7 Irradiance incident on cells integrated in 2D curved modules with different tilt angles between the cells at STC

4.2 Radiation power density on 3D curved PV modules

Figure 8 illustrates an example for the radiation power on each cell of a 3D curved 60-cell module with $\omega_x = 5^\circ$ and $\omega_y = 10^\circ$ when illuminated at STC with 1000 W/m² perpendicular to the center of the module.

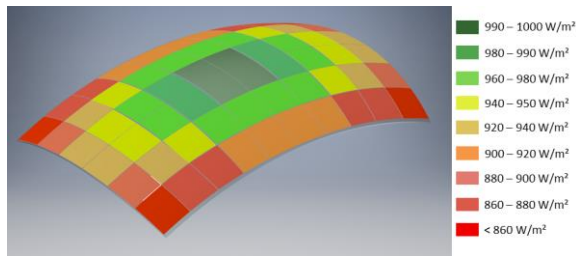


Figure 8 Level of irradiance incident on the cells of a 3D curved module with $\omega_x = 5^\circ$ and $\omega_y = 10^\circ$ at STC

It can be inferred that highest mismatch will occur between the cells in the corners of the module and the cells in the center. The mismatch is a result of the cosine losses which lead to high radiation power reduction at the module edges.

4.3 Energy Yield of 2D curved modules

The results of the energy yield (EY) calculation performed with our analytical model are summarized in Table III.

Table III Results of Energy Yield Simulations

Module type	ω_x [°]	ω_y [°]	EY	
			Series [kWh/a]	Parallel [kWh/a]
Standard module	0	0	353.15	353.15
2D curved modules	2	0	312.4	354.1
	8	0	122.4	342.8
	0	2	335.0	332.8
	0	8	261.0	221.2
3D curved modules	2	2	286.3	332.6
	2	8	220.9	259.1
	8	2	97.9	265.9
	8	8	85.8	221.6

Figure 9 depicts the comparison of the energy yield of 2D curved PV modules and their yield losses compared to the planar module.

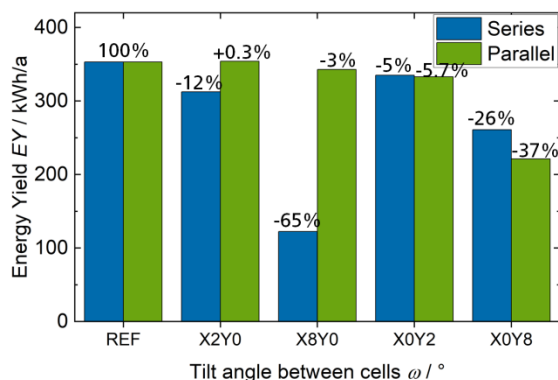


Figure 9 Comparison of the EY of 2D curved modules

The results show that for modules with curvatures over the 10-cell axis it is more advantageous to use parallel interconnection to minimize power losses due to electrical mismatch. The PV module with minor bending angle ($\omega_x = 2^\circ$) and parallel interconnection shows a slight increase in energy yield ($\Delta EY = + 0.3\%$) compared to the standard flat module. The reason for this could be the more favorable tilt angles towards the sun of the strings in the module half that is facing towards the

sun. As the parallel interconnected strings produce power independently of each other the strings with more favorable tilt could lead to higher module power. The module with great bending angle ($\omega_x = 8^\circ$) shows a significant difference between series and parallel interconnection. While the parallel topology reaches 97% of the EY of the planar module, the series interconnected module only reaches 35% of the reference yield. Nevertheless it has to be considered that electrical losses are not considered in these calculations which may reduce overall power output for parallel circuits.

On the contrary, if the module is solely bent over the 6-cell axis high mismatch occurs inside the parallel connected strings which lead to high energy losses up to -37% compared to the flat module. The topology with series interconnection along the 10-cell axis has three string pairs which are interconnected with bypass diodes. The diodes between the string pairs improve the module performance if the module is partly shaded due to the curvature in this case.

4.4 Energy Yield of 3D curved PV Modules

We analyzed 3D curved module designs with slight and great uniform synclastic curvature as well as disparate curvature. The results of the energy yield simulations for 3D curved PV modules are summarized in figure 10.

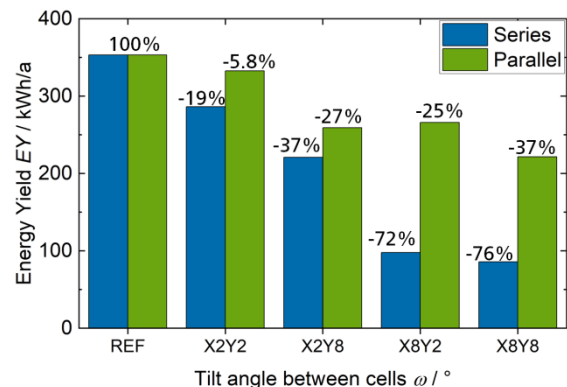


Figure 10 Comparison of the EY of 3D curved PV modules

Overall it can be concluded that 3D curved modules achieve higher energy yield with parallel string interconnection than with series interconnection. This is due to the fact that one module half is mostly facing away from the sun, independent of the sun location. The cells in the “rear part” of the module are shaded when the elevation angle of the sun is equal or lower than the tilt angle of the cell which happens mostly in the morning and evening hours and in the winter months. If one cell in a series interconnected string is completely shaded the output of the string (going from the “front” to the “rear”) equals zero. On the contrary with parallel interconnection, the cells and strings in the “front” deliver power independently from the cells in the “rear” which leads to a significant module output even if the “rear part” of the module is shaded. The tilt angle of the parallel strings in the “front” favors higher yield at low sun level.

Figure 11 depicts a comparison of the monthly energy yield of 3D curved modules with tilt angles of $\omega_x = 8^\circ$

and $\omega_y = 2^\circ$ between the cells with series and parallel interconnection. Furthermore it shows the monthly yield of a planar module with a tilt angle $\beta_{\text{Mod}} = 0^\circ$ as well as the monthly total of global horizontal irradiance.

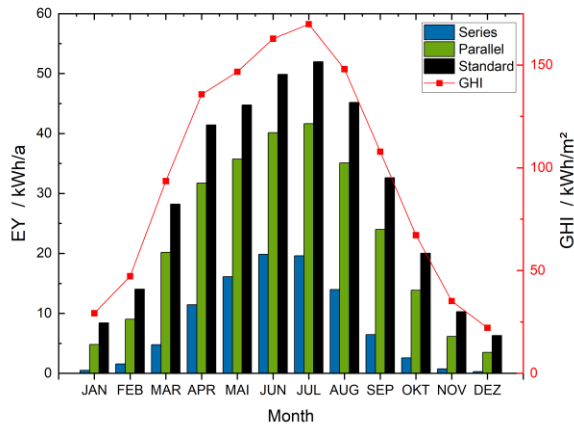


Figure 11 Monthly energy yield of 3D curved PV modules with $\omega_x = 8^\circ$ and $\omega_y = 2^\circ$ compared to standard flat module

Figure 11 supports the assertion that series interconnection of strings in 3D curved modules is particularly disadvantageous in winter months between October and February as almost no output is generated during these months.

Moreover it leads to the conclusion that the occurrence of self-shading of the module is quite high for 3D curved modules with large bending angle as energy yield loss is high for series interconnection. Parallel interconnection of strings yields three times more energy than series interconnection in this case.

5 SUMMARY AND CONCLUSION

In summary, it can be concluded that the interconnection technology has a significant influence on the yearly yield of curved PV modules. In our scenario, the module topology with parallel string interconnection shows better performance against electrical mismatch that occurs due to the inhomogeneous insolation on the module surface. We can conclude that parallel interconnection of strings along the axis of greater curvature will lead to higher energy yields. The solar cells should be interconnected in series to strings along the axis of slighter curvature. However, it has to be mentioned that optical and electrical losses within the module were not considered in this calculation. Optical losses at the front surface will most likely increase the inhomogeneous effects that we see in this study, due to increasing losses at higher incidence angles. While parallel interconnection may be most suitable for our discussed scenarios, there may be other scenarios where series interconnection, in combination with bypass diodes may still lead to highest performance. This strongly depends on the curvature and specific layout but also on the resistive losses within the module.

Furthermore, we have shown that there is a high frequency of occurrence of partial shading in PV modules with 3D contour with great bending angle. Self-shading of the PV module happens mostly in the morning and evening hours as well as in the winter months when the

elevation angle of the sun is low.

The model allows the evaluation of the energy yield potential of curved PV modules considering the angle of curvature between the cells, module orientation and location. Consequently, the elaborated model can be used to predict the energy yield of curved vehicle integrated (VIPV) and building integrated (BIPV) photovoltaic applications.

In addition to that, the model enables to determine the optimum interconnection topology for yield maximization for any curved module design.

6 REFERENCES

- [1] Christoph Kutter, Helen Rose Wilson, Andrea Pfreundt, Martin Heinrich, Harry Wirth, "Light Attenuation Model to Predict Nominal Power of Modules with Light-Scattering Ceramic Printed Front Glasses," in *Proceedings of the 35th European Photovoltaic Solar Energy Conference and Exhibition (EU PVSEC); Brussels, Belgium, 2018*.
- [2] Johannes Eisenlohr, Claudio Ferrara, Benedikt Bläsi, Thomas Kroyer, Oliver Höhn, Martin Heinrich, Ulrich Eitner, Tilmann E. Kuhn, "Highly efficient coloured BIPV modules with anti-glare properties," in *13th Conference on Advanced Building Skins 2018*.
- [3] U. Eitner *et al.*, "Solar Potential on Commercial Trucks: Results of an Irradiance Measurement Campaign on 6 Trucks in Europe and USA," in *Proceedings of the 33rd European Photovoltaic Solar Energy Conference and Exhibition (EU PVSEC)*, Amsterdam, 2017, pp. 2147–2150.
- [4] M. Heinrich *et al.*, "Potential and challenges of vehicle integrated photovoltaics for passenger cars," in.
- [5] C. Kutter, F. Basler, M. Heinrich, and D. H. Neuhaus, "Integrated lightweight, glass-free PV module technology for box bodies of commercial trucks," in.
- [6] H. Hanifi, C. Pfau, J. Schneider, and J. Bagdahn, "A Simulation Based Optical and Electrical Approach to Estimate Energy Yield of Various Designs of Curved Modules," 2016, doi: 10.4229/EUPVSEC20162016-5BV.2.62.
- [7] K. Araki, Y. Ota, and M. Yamaguchi, "Measurement and Modeling of 3D Solar Irradiance for Vehicle-Integrated Photovoltaic," *Applied Sciences*, vol. 10, no. 3, p. 872, 2020, doi: 10.3390/app10030872.
- [8] K. Araki, Y. Ota, and M. Yamaguchi, "Modeling on Unconventional PVs and Their Standardization – Curved Surface, Vehicle-Integration, Multi-Junction Cells, and Static Concentrators,"
- [9] C. Schuss, B. Eichberger, and T. Rahkonen, "A monitoring system for the use of solar energy in electric and hybrid electric vehicles," in *2012 IEEE International Instrumentation and Measurement Technology Conference Proceedings, Graz, Austria, May. 2012 - May. 2012*, pp. 524–527.
- [10] C. Schuss, B. Eichberger, and T. Rahkonen, "Impact of solar radiation on the output power of moving photovoltaic (PV) installations," in *2018*

- IEEE International Instrumentation and Measurement Technology Conference (I2MTC)*, Houston, TX, May. 2018 - May. 2018, pp. 1–6.
- [11] C. Schuss, H. Gall, K. Eberhart, H. Illko, and B. Eichberger, “Alignment and interconnection of photovoltaics on electric and hybrid electric vehicles,” in *2014 IEEE International Instrumentation and Measurement Technology Conference (I2MTC) Proceedings*, Montevideo, Uruguay, May. 2014 - May. 2014, pp. 153–158.
- [12] C. Schuss, T. Kotikumpu, B. Eichberger, and T. Rahkonen, “Impact of dynamic environmental conditions on the output behaviour of photovoltaics,” in pp. 993–998.
- [13] S. A. Kalogirou, “Environmental Characteristics,” pp. 49–762, doi: 10.1016/B978-0-12-374501-9.00002-9.
- [14] <https://solcast.com/historical-and-tmy/>
- [15] https://pvpmc.sandia.gov/applications/pv_lib-toolbox/
- [16] Pfreundt et al. 2020 (*unpublished*)